

Membrane permeability of hydrocarbon-cross-linked peptides

Tzu-Lin Sun, Yen Sun, Chang-Chun Lee and Huey W. Huang*
Department of Physics & Astronomy, Rice University, Houston, Texas 77005, USA

*Corresponding: Huey W. Huang, hwhuang@rice.edu

Abstract

Schafmeister, Po and Verdine (JACS 122, 5891 (2000)) introduced a method utilizing a hydrocarbon linker (“staple”) to stabilize a peptide in a helical configuration. One intended goal of this scheme is to facilitate the delivery of peptide drugs into target cells. Here we investigate whether stapled peptides are intrinsically membrane permeable, by performing a case study on a stapled 12-mer peptide named NYAD-1. We found that the native peptide CAI (an HIV-1 inhibitor) does not bind to lipid bilayers, however NYAD-1 indeed permeates through lipid bilayers even at low solution concentrations. In order to understand the reason for the membrane permeability, we investigated the physical properties of NYAD-1 as a function of bound peptide-to-lipid molar ratio P/L. We found that NYAD-1 spontaneously binds to a lipid bilayer. At low P/L, the peptide primarily binds on the polar-apolar interface with its helical axis parallel to the bilayer that has the effect of stretching the membrane area and thinning the membrane. The membrane thinning reaches its maximum at $P/L \sim 1/15 - 1/12$ in DOPC bilayers. Additional bound peptides has little thinning effect and their helical axes are normal to the plane of bilayers. Thus the stapled peptide has a membrane interaction behavior similar to helical antimicrobial peptides, such as magainin and melittin. We emphasize that not all peptides bind to lipid bilayers in the α -helical form behave this way.

INTRODUCTION

The lipid matrix of a cell membrane provides a hydrophobic barrier that defines the boundary of the cell. An intact membrane is crucial for cell function but it is also a major impediment for the delivery of therapeutic agents into cells. This is so even if the drug enters the cell by endocytosis—in such a case, drug still needs to cross the endosomal membrane. In recent years a new type of drug technology called stapled peptides has been developed and adopted by the pharmaceutical industry. An all-hydrocarbon “staple” cross-links a peptide at i and $i+4$ or $i+7$ position to increase its α -helix propensity (1-7). The rationale for the stapled peptides is three-fold (1): 1) stabilizing the peptide in a configuration that matches the binding site of the protein target, 2) protecting the peptide against proteolytic action and 3) making the peptide membrane permeable. While the functionality and stability of stapled peptides are understandable, it is not clear why the stapled helicity would facilitate cell uptake. Notably these stapled peptides bypass the Lipinski rules which stipulate that the molecular mass of a drug should not exceed 500 daltons (6, 8). Stapled peptides are several times that size, and yet still traffic to the intracellular targets (2, 4, 7). The goal of our study is to investigate first, if the peptides indeed gain membrane permeability by the stapling modification, and second, if so what could be the underlying mechanism for the membrane permeation. We hope to provide a rational basis for the use of this new drug delivery technology. Understanding the mechanism for membrane permeation will facilitate the development of strategies for drug delivery.

We studied a stapled peptide called NYAD-1 based on a 12-mer peptide CAI that has been found to target the capsid of human immunodeficiency virus type 1 (HIV-1). CAI inhibits HIV-1 assembly *in vitro*; however it failed to inhibit HIV-1 in cell culture. The X-ray crystal structure of CAI in complex with the C-terminal domain of capsid (C-CA) revealed that the peptide adopts an α -helical conformation (4, 9). Accordingly Zhang et al. (4) used the hydrocarbon stapling technique (1-3) to convert CAI into a stable helical peptide named NYAD-1. Subsequently the authors showed the anti-HIV-1 activity of NYAD-1 in cell culture and that the stapled peptide indeed targeted the C-CA. However, cellular uptake is not a proof of self-permeation through the membrane. For example, cellular uptake of various cell penetrating peptides has been widely reported, yet the mechanisms of cell penetrating peptides are still being debated (10, 11).

With a fluorescence-labeled NYAD-1 (named NYAD-2) we found that the peptide indeed permeates across lipid bilayers. In order to understand what properties of the peptide enable the membrane permeability, we studied NYAD-1 mixed in lipid bilayers as a function of peptide-to-lipid ratio. We compare the results with antimicrobial peptides and amyloid precursor peptides. We discuss the important properties of NYAD-1 that make the peptide membrane permeable.

EXPERIMENT

Materials and sample preparation

NYAD-1 is H - Ile - Thr - Phe - X - Asp - Leu - Leu - X - Tyr - Tyr - Gly - Pro - NH₂ [with special cyclization to get double bond, X= (S) - alpha - (2'-pentenyl)alanine] (4). NYAD-1 and CAI (H-Ile-Thr-Phe-Glu-Asp-Leu-Leu-Asp-Tyr-Tyr-Gly-Pro-NH₂) were synthesized by CPC Scientific Inc (San Jose, CA) under the supervision of Xiaohu Tong, one of the authors of (4). NYAD-2 is FITC - (beta - Ala) - Ile - Thr - Phe - X - Asp - Leu - Leu - X - Tyr - Tyr - Gly - Pro - NH₂ (with special cyclization to get double bond, X= (S) - alpha - (2'-pentenyl)alanine; FITC = fluorescein isothiocyanate) synthesized by AnaSpec (Fremont, CA). The chemical structures of NYAD-1 and NYAD-2 (4) are reproduced in Fig. 1. 1,2-dioleoyl-sn-glycero-3-phosphocholine (DOPC), 1,2-dioleoyl-sn-glycero-3-phosphoethanolamine-N-(lissamine rhodamine B sulfonyl) (Rh-DOPE), and 1,2-dioleoyl-sn-glycero-3-phosphoethanolamine-N-(7-nitro-2-1,3-benzoxadiazol-4-yl) (NBD-DOPE) were purchased from Avanti Polar Lipids (Alabaster, AL). Texas Red sulfonyl chloride (TRsc) (MW 625), Texas Red dextran (TRD) (MW 10000) and calcein (MW 623) were purchased from Invitrogen (Grand Island, NY). Fluorescein PEG (MW 1000), was purchased from NANOCS (Boston, MA). All other chemicals were purchased from Sigma-Aldrich (St. Louis, MO) and were used without further purification. All experiments were performed in room temperature ~25° C unless specified otherwise.

Giant unilamellar vesicles (GUVs) were produced by the electroformation method (12) in a production chamber containing a GUV interior solution. The solution includes ~200 mM sugar (sucrose or glucose) to control the osmolality, a pH buffer and solution dyes if necessary. A typical GUV experiment was performed with GUVs containing ~200 mM sucrose inside, in an outside solution of ~200 mM glucose. The refractive index contrast between sucrose and glucose makes the GUVs visible and the density contrast makes the GUVs sink to the bottom of the solution for the ease of manipulation. The osmolalities of the solutions used for the GUV interior and GUV exterior were measured separately by a Wescor Model 5520 dew-point Osmometer (Wescor, Logan, UT). Equi-osmolality between the inside and outside of the GUV was the initial condition in all GUV experiments. To produce GUVs, DOPC or DOPC and 0.5% molar ratio of Rh-DOPE (for clear imaging) were dissolved in 1:1 (v/v) tetrafluoroethylene and chloroform. The lipid solution (~0.05 mg lipid) was deposited onto two ITO coated glass cover slips. After drying under vacuum, an o-ring was sandwiched between the two ITO slips and the gap was filled with the interior solution. 3 V ac at 10 Hz was applied between the two ITO electrodes for 2 h. Subsequently the frequency was adjusted to 5 Hz for 10 mins and followed by 1 Hz for 10 mins. This electroformation method has been shown to produce unilamellar large vesicles (12). The GUV suspension was then gently collected in a glass vial (reservoir). The vesicles were used within 24 hrs of production.

Aligned multilamellae of peptide/lipid mixtures were prepared by first dissolving the peptide and lipid at a chosen molar ratio, P/L, in 1:1 (v/v) tetrafluoroethylene and chloroform. The mixture was uniformly spread on a thoroughly cleaned fused-quartz substrate (0.018 mg peptide on a 1 cm² quartz plate for $P/L > 1/30$; 0.3 mg of lipid on a 1 cm² plate for $P/L \leq 1/30$). After the

solvent evaporated in vacuum, the sample was hydrated with saturated water vapor in 37° C oven overnight. The results were well-aligned parallel bilayers, as proven by x-ray diffraction. During the experiment, the samples were housed in a temperature humidity chamber in which the hydration level of the sample was controlled by the relative humidity (RH) of water vapor (13).

Aspirated GUV experiment

The experimental setup for aspirated GUV experiment was described in Sun et al (14). Before the experiment, micropipettes (with inner diameter 16-20 μm) and the walls of sample chambers were coated with 0.5% bovine serum albumin in order to dissipate the charge on the glass surface and then washed extensively with water. The micropipette was connected to an oil-filled U tube where a negative pressure was produced and controlled by reference to the atmosphere pressure (15).

A selected GUV (diameter $\sim 30\text{-}70 \mu\text{m}$) in the reservoir was aspirated at a low constant negative pressure ($\sim 100 \text{ Pa}$ producing a membrane tension $\sim 0.4 \text{ mN/m}$) by a micropipette, and transferred via a transfer pipe (14) to an observation chamber where the solution contained the peptide. Note that CAI, NYAD-1 or NYAD-2 was added to the solution by first dissolving in DMSO (the DMSO concentration in the experimental chamber was 2 to 7 mM). It is known that DMSO permeates through lipid bilayers (16). In order to avoid the effect of DMSO on osmolality balance (16), the same concentration of DMSO was also added to the interior solution, so that the osmolality of the solution in the observation chamber was the same as in the GUV interior solution. The response of the GUV to the peptide binding was observed by a conventional inverted widefield microscope (IX81, Olympus, Tokyo, Japan) and recorded by a Hamamatsu Photonics digital CCD Camera (model C10600-10B) (Hamamatsu City, Japan), or by a confocal microscopy (Nikon C1 si-LU4A confocal spectral imaging system and Nikon C2 confocal laser point scanning system—Tokyo, Japan) with 488nm/561nm lasers (OBIS/Sapphire, Coherent, Santa Clara, CA).

In response to peptide binding, a GUV can potentially change its membrane area A and volume V . The GUV protrusion inside the micropipette serves as an amplifier for the measurement of such changes. From the microscopic images, L_p the length of the protrusion, R_p the radius of the micropipette, and R_v the radius of the GUV were carefully measured. Then it is straightforward to show $\Delta A = 2\pi R_p \Delta L_p + 8\pi R_v \Delta R_v$, and $\Delta V = \pi R_p^2 \Delta L_p + 4\pi R_v^2 \Delta R_v$ (17). If there is no molecular leakage and as long as the inside and outside of the GUV have the same osmolality, there should be no change of volume. Under the condition $\Delta V = 0$, ΔL_p is directly proportional to ΔA : $\Delta A = 2\pi R_p (1 - R_p/R_v) \Delta L_p$.

On the other hand, if peptides induce formation of transmembrane pores, the influx of glucose will be greater than the efflux of sucrose through the pores, because sucrose is approximately two times as large as glucose. The resultant osmolality imbalance induces a net water influx, causing a volume increase in the GUV (18). (Conversely if sucrose and glucose

were exchanged, the GUV volume decreased (14).) If the membrane area is constant, the relation between ΔL_p and ΔV is $\Delta V = -\pi R_p (R_v - R_p) \Delta L_p$. Thus if peptides induce pores in the membrane, the GUV protrusion length would decrease, $\Delta L_p < 0$, after the peptide binding has reached equilibrium (18, 19).

GUV Leakage experiment

For leakage experiment, the GUV interior solution also contained 30 μM calcein and 50 μM TRD10000. Two observation chambers containing the same solution 190 mM glucose and 10 mM HEPES pH 7 were set side by side. About 10 μL of the GUV suspension was injected into the first observation chamber and well-mixed with the solution in the chamber by stirring. About ten GUVs were transferred from the first to the second chamber via a transfer pipe. The purpose of this two-chamber procedure was to dilute the untrapped calcein and TRD in the solution external to the GUVs. In the second chamber, the GUVs settled at the bottom due to the density differential and were observed by a widefield microscope. The effect of peptide-induced leakage was observed by slowly injecting a small amount of exterior solution containing NYAD-1 into the chamber until the peptide concentration equal to 25 μM . Slow injection (for about 30 s) was necessary so as not to create a flow in the observation chamber.

Membrane permeation experiment

We used FITC labeled NYAD (called NYAD-2) to observe membrane permeation. Like many fluorescent dyes, the fluorescence intensity of NYAD-2 is pH dependent. In particular, we found that the intensity at pH 9 is 1.78 times higher than at pH 7. We decided to use this property to help measuring the intensity of permeated NYAD-2 inside the GUV.

The permeation experiment was performed as follows. The interior solution for GUV production was 190 mM sucrose, 10 mM Tris at pH 9, 10 μM TRsc and 2.82mM DMSO. Two chambers each contained 190 mM glucose, 10 mM Tris at pH 7 and 2.82 mM DMSO were set side by side, one for control and one for observation. Only the observation chamber contained 2 μM NYAD-2. A GUV aspirated from the production chamber was first transferred to the control chamber to dilute the untrapped TRsc in the exterior solution, and then transferred to the observation chamber for observation under a confocal microscope. The image was recorded in two channels: 488 nm for FITC and 561 nm for TRcsc. The recording time was 0.5 s every minute to avoid excessive photobleaching. A negative control was performed with the same conditions with NYAD-2 replaced by fluorescein PEG (1000).

For pH 9 experiment, GUVs were produced in a solution containing 190mM sucrose, 20uM TRsc, 7 mM DMSO and 10 mM Tris at pH 9. The solution in the observation chamber contained 190 mM glucose, 2 μM NYAD-2, 7 mM DMSO, 10 mM Tris at pH9. After GUVs were introduced into the observation chamber, the chamber was sealed to prevent water evaporation. This was necessary for a long permeation time. The images were taken every hour manually by refocusing the microscope because of the slight movement of the GUV.

The fluorescence intensities are corrected as follows. A background intensity from the confocal system, in the absence of the dye but with the same laser power, is subtracted from every intensity reading—this intensity is B . The solution dye intensity, I_O , outside the GUV was practically constant (with negligible photobleaching). This is because there was only one GUV (or ~ 10 GUVs in the case pH 9 experiment) in a chamber of $\sim 700 \mu\text{L}$; the total number of bound NYAD-2 is less than 10^{-6} (or 10^{-5}) of the total in solution. Because of the imperfection of confocality, there is an influence of the dye on the GUV surface to the interior fluorescence intensity. This was estimated by comparing the interior intensities of GUVs with and without lipid dye (NBD-DOPE) on the surface. The interior intensity is increased by 4% of the intensity averaged over the GUV surface, I_S . Similarly the interior intensity is influenced by the external solution intensity which was estimated by the interior reading with fluorescein PEG (1000) outside the GUV. The interior reading is 20% of the external reading. Thus the intensity of GUV interior, I_I , is corrected by 1) the system background, 2) the effect of surface intensity, and 3) the effect of outside intensity: $I_I^c = I_I - B - 0.04I_S - 0.2I_O$. The corrected solution dye intensity outside of the GUV is $I_O^c = I_O - B$.

X-ray diffraction experiment

Multilamellar samples were measured in a temperature-humidity chamber (13). ω -2 θ diffraction was collected on a four-circle Huber goniometer (Huber Diffraktionstechnik, Rimsting, Germany), with a vertical line-focused Cu K_α source ($\lambda=1.542 \text{ \AA}$) operating at 35 kV and 15–30 mA. The incident beam was collimated by a horizontal soller slit and two vertical slits on the front and the back sides of the soller slit. The horizontal and vertical divergences of the incident beam were 0.23° and 0.3° , respectively. The diffracted beam first passed through a vertical slit and then was discriminated by a bent graphite monochromator (selected for 1.542 \AA) before entering a scintillation detector. Thus the detector excluded Compton scattering, fluorescence and most of the X-rays from air scattering. This diffractometer was designed to minimize the background signal, thus allowing the measurement of high diffraction orders.

Before the measurement, the aligned multilayer sample was carefully positioned at the center of the X-ray beam and was oriented so that $\omega = 0^\circ$ and $\theta = 0^\circ$ coincided. We have established an elaborate routine for positioning and orienting the sample as described in Wu et al. (20). A two-dimensional ω - θ scan around the second or the third Bragg order was used to check the alignment of the ω -angle and the mosaic of the multilayers alignment. Typically the FWHM (full width half maximum) of the peak on the ω axis (of the ω - θ scan) was 0.2 - 0.3° (example in (21)). Once the sample was properly positioned and aligned on the diffractometer, each ω -2 θ scan was performed from $\omega=0.5^\circ$ to $\omega=7.5^\circ$ with a step size of $\Delta\omega=0.01^\circ$. An attenuator was used to prevent the first-order Bragg peak from saturating the detector. The scan was repeated 2–3 times at each of several hydration levels and averaged at each hydration level for data analysis. Measurements at several hydration levels were for the purpose of phase determination by the swelling method. Only the results of 98-100 % RH are reported. (Note that the readings

of commercial humidity sensors are not accurate above 98% RH; we used the maximum RH above which the membrane samples would flow.)

The procedure of data reduction was described in many of our previous works (22, 23). Briefly, the measured diffraction intensity was first corrected for the attenuator absorption and for the detector's dead-time factor. After removing the background, data were corrected for sample absorption and diffraction volume. The integrated peak intensities were then corrected for the polarization and the Lorentz factors. The relative magnitude of the diffraction amplitude was the square-root of the integrated intensity. With their phases determined by the swelling method, the diffraction amplitudes were used to reconstruct the electron density profile of the bilayer. Across the bilayer profile, the phosphate peak to phosphate peak distance (PtP) was measured for the bilayer thickness. Measurements by the above described procedure have been applied to various peptide-lipid mixtures for more than a decade, e.g., (20, 21, 23).

Oriented Circular Dichroism (OCD)

CD spectra were measured in a Jasco (Tokyo, Japan) J-810 Spectropolarimeter. Aligned multilamellar samples of NYAD-1 in DOPC bilayers were kept fully hydrated in a humidity chamber with quartz windows. The substrates were oriented normal to the incident light for the measurement of OCD (24). Each sample was measured at least 5 times and averaged. The background spectrum for each sample was measured for the same amount of lipid on the same substrate. After the background correction, the spectra of different *P/L* were normalized by the amount of peptide.

For comparison, a solution CD of NYAD-1 was measured in Tris buffer pH 8 in the presence of 35% (v/v) acetonitrile at a final peptide concentration of 424 μ M (following the protocol given in (4)). (Note that DMSO absorbs UV, not usable for CD measurement.)

RESULTS

(1) Aspirated GUV experiment

Aspirated GUV experiment is useful for understanding the general behavior of a new membrane-acting molecule. To begin with, if the molecule binds to lipid bilayers, we can expect an expansion of the membrane area. The consequence of molecular binding may vary. The molecule could simply incorporate into the lipid bilayer, e.g., curcumin(16). The molecule could form pores in the membrane, e.g., melittin (19). The molecule could turn into aggregates, e.g., penetratin (25). The molecule could extract lipid molecules from the bilayer, e.g., tea catechin (14). These general characteristics of interaction with membranes have been shown for a great variety of lipid compositions, with the only differences in the *P/L* dependence (26). Thus we have arbitrarily chosen DOPC for our investigation. The initial experiment with an aspirated GUV was to provide a qualitative understanding of how NYAD interacts with membranes. We observed what happened to the membrane exposed to NYAD. Equally important was what did not happen to the GUV, for example peptide-lipid aggregates on the GUV surface.

Fig. 1 shows separately the responses of a DOPC GUV to CAI, NYAD-1 and NYAD-2 all at the same concentration 8 μM in pH 7 solutions. There was no indication of CAI binding to the GUV over a long time (Fig. 1A). The very slow increase of the protrusion length was the same as in a control run with no peptide (Fig. 1D). The background increase (in the absence of peptides) was caused by a slow increase of osmolality in the exterior solution due to water evaporation. A higher osmolality in the exterior solution caused an efflux of water from the GUV. A decrease of GUV volume at constant membrane area caused an increase of the protrusion length. This background protrusion length increase is added to the protrusion length increase caused by peptide binding. We normally design our experiment to finish within a few mins, so as to avoid this complication (for example, using anionic lipids to increase the binding rate to cationic peptides). Here, we let the experiment to last for 30 mins to make sure there is no membrane binding by CAI. The experiment with CAI was repeated many times at different peptide concentrations (highest 40 μM) with the same result, all similar to control runs. The conclusion is that CAI has negligible binding affinity to lipid bilayers.

In the presence of 8 μM NYAD-1, the protrusion length increased and reached a maximum within 15 s (Fig. 1B and 1E). This membrane area increase implies peptide binding. After reaching the maximum, the protrusion length decreased indicating that pores were formed in the membrane as explained in the Experiment section. Although the cause of the protrusion length decrease was due to pore formation, the beginning of pore formation was not coincidental with the point of maximum protrusion length. Because of the continuing peptide binding which continued to increase the protrusion length, the protrusion length did not immediately decrease as soon as pores appeared.

The same experiment was repeated for NYAD-2 (Fig. 1C) to show that the FITC label on NYAD-1 did not alter the peptide's characteristic property (Fig. 1E and 1F). The modification by the FITC label slowed the action of the peptide considerably, indicating a lower binding affinity to the bilayer (note the time scale). Nevertheless NYAD-2 also caused the protrusion length increase to a maximum followed by a steady decrease, showing its pore forming capability.

(2) Leakage experiment

This experiment was performed to confirm the observation of pore formation in aspirated GUV experiments. Fig. 2 demonstrates molecular leakage induced by NYAD-1 at high concentrations. A GUV containing green dye calcein (MW 623) and red dye TRD (MW 10000) was transferred to the observation chamber. NYAD-1 dissolved in the external solution was slowly injected into the observation chamber until its final concentration was 25 μM . After a while both dyes were observed to leak out, while the GUV membrane remained intact (Fig. 2). The time of leakage depended on the position of the injector relative to the GUV and the speed of injection.

Understandably the leakage of calcein was faster than TRD10000 due to the difference in molecular weight. When the same leakage experiment was performed with antimicrobial peptide

magainin, the pores at first allowed both large and small dye molecules to leak out but after a while only small molecules continued to leak out, implying a pore size reduction with time (27). It is not clear from our leakage curves whether the large dye would leak out completely. The pore size kinetics was not pursued, because it is probably of no interest to the therapeutic use of NYAD-1 at much lower concentrations.

(3) NYAD permeation experiment

Because NYAD peptide forms pores at high concentrations, the permeation experiment was conducted at a low peptide concentration, 2 μM , to avoid pore formation. However, the fluorescence intensity of NYAD-2 at this concentration was too weak for the permeation measurement. We tested and found that the fluorescence intensity of NYAD-2 at pH 9 is 1.78 times higher than at pH 7. To make use of this pH effect, we produced GUVs with a pH 9 solution in the lumen and performed the permeability experiment in pH 7 solutions.

An aspirated GUV was first imaged in the control chamber (which contained no NYAD-2) right before it was transferred to the observation chamber. It took ~ 1.5 min to readjust the confocal focus after the transfer. Therefore the first fluorescence measurement was taken ~ 1.5 min after the GUV was exposed to 2 μM NYAD-2. The time sequence of images is shown in Fig. 3A. The protrusion length increased without any sign of decrease, indicating peptide binding without molecular leakage. The absence of molecular leakage was reconfirmed by the constant intensity of TRsc inside the GUV (Fig. 3B). The steady increase of the FITC fluorescence intensity inside the GUV clearly indicates permeation of NYAD-2 through the GUV membrane. However, after the normalization by the effect of pH 9 (i.e., dividing the corrected inside intensity by 1.78), we were surprised to find the normalized intensity of NYAD-2 inside the GUV greater than the intensity outside after ~ 30 min (Fig. 3B).

This unusual phenomenon could be explained by a possible pH-effect on the concentration dependence of the chemical potential. If the peptide can permeate through the membrane, the chemical potential of NYAD-2 will approach an equal value inside and outside. However the concentration dependence of the chemical potential could be different for pH 7 and pH 9.

We also performed a permeation experiment with a pH 9 solution both inside and outside of GUV, so that there was no differential pH effect. Fig. 4 shows the result. Clearly the fluorescence intensity of NYAD-2 inside the GUV increased with time and it approached $\sim 60\%$ of the outside intensity after ~ 7 h, while the fluorescence intensity of the interior dye TRsc was constant. NYAD-2 permeated through the lipid bilayer without causing molecular leakage. We did not feel necessary to continue this manual experiment any longer to prove the permeation of NYAD-2. For a negative control, the pH 7-pH 9 permeability experiment was performed with fluorescein PEG (1000) replacing NYAD-2. As expected, no fluorescein PEG was detected inside the GUV.

(4) Membrane thinning by NYAD-1 binding

Electron density profiles obtained by X-ray diffraction show that the peptide-lipid mixtures formed well-defined lipid bilayers (Fig. 5 A,B). The electron density of the peptides did not show up in the diffraction-constructed profiles, because the peptide positions were not correlated from bilayer to bilayer (diffraction is the result of electron density correlations (28)). The most important effect of peptide binding is measured by the phosphate peak to phosphate peak distance across the bilayer (PtP). PtP is a measure of the bilayer thickness. It decreases more or less linearly with P/L up to a value P/L^* between 1/15 and 1/12, and levels off for $P/L > P/L^*$ (Fig. 5C). Previous studies with antimicrobial peptides (AMPs) (29, 30) showed that AMPs caused a linear decrease of PtP with P/L and followed by a PtP leveling off, similar to NYAD-1. Neutron in-plane scattering showed that transmembrane pores were formed in the bilayers for $P/L > P/L^*$ but no pores were detected for $P/L < P/L^*$ (31-33). Thus for AMPs, P/L^* is the threshold concentration for pore formation.

Membrane thinning in proportion to P/L implies that peptides bind on the bilayer interface. Due to the near incompressibility of the hydrocarbon volume in the chain region of lipid bilayer (34), the area expansion is accompanied by a corresponding membrane thinning. Thus the linear thinning detected by X-ray corresponds to the initial membrane expansion detected in the aspirated GUV experiment.

(5) OCD measurement

Although NYAD-1 is only 12 amino-acid long, its solution CD is no different from a normal α -helical spectrum (Fig. 6). Its OCD spectra are also similar to that of longer peptides (Fig. 6). The method of OCD was explained in great detail in Wu et al. (24). The most prominent feature for α -helices is the orientation dependence of the π - π^* transition near 208 nm. The electric transition dipole for this band is polarized along the helical axis, therefore the band magnitude is largest when the helices are perpendicular to the light or parallel to the plane of membrane and vanishes when the helices are in the direction of light or perpendicular to membrane (24). The magnitude of the n - π^* transition near 224 nm also decreases (but not vanishes) as the helices change from parallel to perpendicular orientation relative to the plane of membrane. Fig. 6 shows that for all values of $P/L \leq 1/20$, the OCD spectra of NYAD-1 are identical and have the largest 208 nm amplitude (compared with the OCD at higher P/L's), consistent with the peptide helices being parallel to the bilayer at low P/L's. The decrease of 208 nm amplitude for $P/L \geq 1/15$ indicates that a fraction of NYAD-1 helices changed to normal orientation, and this fraction increased with P/L. The transition point where a fraction of helices begin to change orientation from parallel to perpendicular is between $P/L=1/20$ and $1/15$, which is reasonably close to the membrane thinning transition point (P/L between 1/15 and 1/12) where membrane thinning levels off (Fig. 5C). In many other peptide experiments, we found that these two transition points were in agreement within experimental errors (29, 30, 35).

Note that a solution CD is the orientational average of the OCD spectra and is equivalent to a mixture of 1/3 of helices normal to the bilayer and 2/3 of helices parallel to the bilayer (this

was proven both theoretically and experimentally in (24)). The shape of the solution CD is between the OCD spectra at $P/L=1/15$ and $1/10$.

DISCUSSION

The same experimental methods have been used in the past to discover at least four different types of membrane-active molecules. Our intention is to compare NYAD-1 with them. Curcumin induces a non-linear membrane thinning as a function of P/L ; its binding states are a combination of interfacial state and chain insertion state; it has no other effects on the membrane (16, 36). Tea catechin induces a linear membrane thinning; it binds only to the interface of membranes but also solubilizes the lipid molecules (14). Amyloid peptide penetratin binds to membranes as an α -helix and induces a linear membrane thinning until P/L reaches a critical value P/L^* ; additional peptide binding ($P/L > P/L^*$) would turn the peptides into β -sheet aggregates and come off the external surface of GUV (25, 35). AMPs induces a linear membrane thinning until P/L reaches P/L^* ; additional peptide binding ($P/L > P/L^*$) causes pore formation. Clearly the membrane interaction behavior of NYAD-1 is closely similar to AMPs.

First, we found that both NYAD-1 and NYAD-2 bound to the lipid bilayer and expanded the membrane area, whereas the native peptide CAI did not. To distinguish whether the peptide binding is on the bilayer's polar-apolar interface or into the lipid chain region, we performed X-ray diffraction experiment. The result showed that the membrane thickness decreased linearly in proportion to P/L . This implies that the initial binding is on the bilayer interface. However, when P/L exceeds P/L^* , the membrane thinning levels off, exactly in the same manner as AMPs. The leakage experiment showed that NYAD-1 formed pores in the membrane but left the GUV intact.

A method for measuring membrane permeability

To detect the membrane permeability of NYAD, we used the dye-labeled NYAD-2 which we have shown to have the same membrane interaction as NYAD-1, i.e., binding to the membrane and causing membrane leakage at high P/L . To overcome the weak fluorescence intensity in low concentrations (e.g., $2 \mu\text{M}$), we exploited the pH dependence of FITC fluorescence whose intensity at pH 9 is 1.78 times higher than at pH 7. A previous experiment by Zhou and Raphael (37) has showed that there was little change in the bilayer elastic properties between pH 7 and pH 9.

The permeability experiment was performed by introducing GUVs containing a pH 9 solution into a solution of NYAD-2 at pH 7. The result (Fig. 3A) clearly shows that NYAD-2 peptides permeated through the membrane, while the integrity of the membrane was assured by no decrease of the GUV protrusion length (see the experimental section on aspirated GUVs) and no leakage of TRsc. Permeation was also demonstrated with pH 9 solutions both inside and outside of the GUV, in the absence of differential pH effect. This method of membrane permeability measurement could be useful for other membrane-active molecules.

Membrane-bound states and membrane permeability

At low concentrations, the membrane bound state of NYAD-1 is on the bilayer interface. Nevertheless the peptide can translocate across the bilayer. Thus we conclude that the hydrocarbon-stapling has imparted three essential characteristics to NYAD-1 that are relevant to its membrane permeability. First, the hydrocarbon link provides an amphiphathic molecular surface to the otherwise hydrophilic peptide. CAI has negligible binding affinity to lipid bilayers, whereas NYAD-1 has a strong affinity for membrane binding. Second, NYAD-1 has a membrane interacting property similar to AMPs. Third, the hydrocarbon stapling prevents the peptide from turning into β -sheet-aggregates; the possibility of forming amyloids could deprive a peptide of its membrane permeability, as in the case of penetratin (25, 35).

ACKNOWLEDGMENTS

This work was supported by NIH (US) Grant GM55203 and by the Robert A. Welch Foundation Grant C-0991.

References

1. Schafmeister, C. E., J. Po, and G. L. Verdine. 2000. An All-Hydrocarbon Cross-Linking System for Enhancing the Helicity and Metabolic Stability of Peptides. *Journal of the American Chemical Society* 122:5891-5892.
2. Walensky, L. D., A. L. Kung, I. Escher, T. J. Malia, S. Barbuto, R. D. Wright, G. Wagner, G. L. Verdine, and S. J. Korsmeyer. 2004. Activation of apoptosis in vivo by a hydrocarbon-stapled BH3 helix. *Science* 305:1466-1470.
3. Bernal, F., A. F. Tyler, S. J. Korsmeyer, L. D. Walensky, and G. L. Verdine. 2007. Reactivation of the p53 tumor suppressor pathway by a stapled p53 peptide. *J Am Chem Soc* 129:2456-2457.
4. Zhang, H., Q. Zhao, S. Bhattacharya, A. A. Waheed, X. Tong, A. Hong, S. Heck, F. Curreli, M. Goger, D. Cowburn, E. O. Freed, and A. K. Debnath. 2008. A cell-penetrating helical peptide as a potential HIV-1 inhibitor. *J Mol Biol* 378:565-580.
5. Kutchukian, P. S., J. S. Yang, G. L. Verdine, and E. I. Shakhnovich. 2009. All-atom model for stabilization of alpha-helical structure in peptides by hydrocarbon staples. *Journal of American Chemical Society* 131:4622-4627.
6. Arora, P. S., and A. Z. Ansari. 2009. Chemical biology: A Notch above other inhibitors. *Nature* 462:171-173.
7. Moellering, R. E., M. Cornejo, T. N. Davis, C. Del Bianco, J. C. Aster, S. C. Blacklow, A. L. Kung, D. G. Gilliland, G. L. Verdine, and J. E. Bradner. 2009. Direct inhibition of the NOTCH transcription factor complex. *Nature* 462:182-188.
8. Lipinski, C. A., F. Lombardo, B. W. Dominy, and P. J. Feeney. 2001. Experimental and computational approaches to estimate solubility and permeability in drug discovery and development settings. *Adv Drug Deliv Rev* 46:3-26.
9. Ternois, F., J. Sticht, S. Duquerroy, H. G. Krausslich, and F. A. Rey. 2005. The HIV-1 capsid protein C-terminal domain in complex with a virus assembly inhibitor. *Nat Struct Mol Biol* 12:678-682.
10. Yang, S. T., E. Zaitseva, L. V. Chernomordik, and K. Melikov. 2010. Cell-penetrating peptide induces leaky fusion of liposomes containing late endosome-specific anionic lipid. *Biophys. J.* 99:2525-2533.
11. Madani, F., S. Lindberg, U. Langel, S. Futaki, and A. Graslund. 2011. Mechanisms of cellular uptake of cell-penetrating peptides. *J Biophys* 2011:414729.
12. Angelova, M. I. 2000. Liposome Electroformation. In *Giant Vesicles*. P. L. Luisi, and P. Walde, editors. John Wiley & Sons, Chichester. pp. 27-36.
13. Yang, L., and H. W. Huang. 2003. A rhombohedral phase of lipid containing a membrane fusion intermediate structure. *Biophys J* 84:1808-1817.
14. Sun, Y., W. C. Hung, F. Y. Chen, C. C. Lee, and H. W. Huang. 2009. Interaction of tea catechin (-)-epigallocatechin gallate with lipid bilayers. *Biophys J* 96:1026-1035.
15. Fygenson, D. K., M. Elbaum, B. Shraiman, and A. Libchaber. 1997. Microtubules and vesicles under controlled tension. *Phys. Rev. E* 55:850-859.
16. Sun, Y., C. C. Lee, W. C. Hung, F. Y. Chen, M. T. Lee, and H. W. Huang. 2008. The bound states of amphipathic drugs in lipid bilayers: study of curcumin. *Biophys J* 95:2318-2324.
17. Kwok, R., and E. Evans. 1981. Thermoelasticity of large lecithin bilayer vesicles. *Biophys J* 35:637-652.
18. Longo, M. L., A. J. Waring, L. M. Gordon, and D. A. Hammer. 1998. Area expansion and permeation of phospholipid membrane bilayer by influenza fusion peptides and melittin. *Langmuir* 14:2385-2395.
19. Lee, M. T., W. C. Hung, F. Y. Chen, and H. W. Huang. 2008. Mechanism and kinetics of pore formation in membranes by water-soluble amphipathic peptides. *Proc Natl Acad Sci U S A* 105:5087-5092.

20. Wu, Y., K. He, S. J. Ludtke, and H. W. Huang. 1995. X-ray Diffraction Study of Lipid Bilayer Membrane Interacting with Amphiphilic Helical Peptides: Diphytanoyl Phosphatidylcholine with Alamethicin at Low Concentrations. *Biophys J* 68:2361-2369.
21. Weiss, T. M., P. C. van der Wel, J. A. Killian, R. E. Koeppe, 2nd, and H. W. Huang. 2003. Hydrophobic mismatch between helices and lipid bilayers. *Biophys J* 84:379-385.
22. Olah, G. A., H. W. Huang, W. H. Liu, and Y. L. Wu. 1991. Location of ion-binding sites in the gramicidin channel by X-ray diffraction. *J Mol Biol* 218:847-858.
23. Harroun, T. A., W. T. Heller, T. M. Weiss, L. Yang, and H. W. Huang. 1999. Experimental evidence for hydrophobic matching and membrane-mediated interactions in lipid bilayers containing gramicidin. *Biophys J* 76:937-945.
24. Wu, Y., H. W. Huang, and G. A. Olah. 1990. Method of oriented circular dichroism. *Biophys J* 57:797-806.
25. Sun, Y., C. C. Lee, T. H. Chen, and H. W. Huang. 2010. Kinetic Process of beta-Amyloid Formation via Membrane Binding. *Biophys J* 99:544-552.
26. Lee, M. T., W. C. Hung, F. Y. Chen, and H. W. Huang. 2005. Many-body effect of antimicrobial peptides: on the correlation between lipid's spontaneous curvature and pore formation. *Biophys J* 89:4006-4016.
27. Tamba, Y., H. Ariyama, V. Levadny, and M. Yamazaki. 2010. Kinetic pathway of antimicrobial peptide magainin2 induced pore formation in lipid membranes. *J. Phys. Chem. B* 114:12018-12026.
28. Warren, B. E. 1990. X-ray Diffraction. Dover Publications,, Mineola, N.Y.; pp. 41-47, 51-54.
29. Huang, H. W. 2006. Molecular mechanism of antimicrobial peptides: the origin of cooperativity. *Biochim Biophys Acta* 1758:1292-1302.
30. Lee, C. C., Y. Sun, S. Qian, and H. W. Huang. 2011. Transmembrane pores formed by human antimicrobial peptide LL-37. *Biophys J* 100:1688-1696.
31. He, K., S. J. Ludtke, D. L. Worcester, and H. W. Huang. 1996. Neutron scattering in the plane of membranes: structure of alamethicin pores. *Biophys J* 70:2659-2666.
32. Ludtke, S. J., K. He, W. T. Heller, T. A. Harroun, L. Yang, and H. W. Huang. 1996. Membrane pores induced by magainin. *Biochemistry* 35:13723-13728.
33. Yang, L., T. A. Harroun, T. M. Weiss, L. Ding, and H. W. Huang. 2001. Barrel-stave model or toroidal model? a case study on melittin pores. *Biophys J* 81:1475-1485.
34. Seemann, H., and R. Winter. 2003. Volumetric properties, compressibilities, and volume fluctuations in phospholipid-cholesterol bilayers. *Z. Phys. Chem.* 217:831-846.
35. Lee, C. C., Y. Sun, and H. W. Huang. 2010. Membrane-mediated peptide conformation change from alpha-monomers to beta-aggregates. *Biophys J* 98:2236-2245.
36. Hung, W. C., F. Y. Chen, C. C. Lee, Y. Sun, M. T. Lee, and H. W. Huang. 2008. Membrane-thinning effect of curcumin. *Biophys J* 94:4331-4338.
37. Zhou, Y., and R. M. Raphael. 2007. Solution pH alters mechanical and electrical properties of phosphatidylcholine membranes: relation between interfacial electrostatics, intramembrane potential, and bending elasticity. *Biophys J* 92:2451-2462.

FIGRUE LEGENDS

Figure 1 The sequences of CAI, NYAD-1 and NYAD-2 are reproduced from (4). An aspirated GUV of DOPC (and 0.5% molar ratio of Rh-DOPE) was introduced into a solution containing 8 μM CAI (A), 8 μM NYAD-1 (B) or 8 μM NYAD-2 (C) at pH 7. The length of the GUV protrusion into the micropipette, L_p , was measured at regular time intervals. For the purpose of comparison, ΔL_p was converted to the fractional area change $\Delta A/A$ by the relation $\Delta A = 2\pi R_p(1 - R_p/R_v)\Delta L_p$. (A) With CAI, the protrusion length increase is similar to the control runs without peptides, as shown in (D). (B)/(C) With NYAD-1/NYAD-2, the protrusion length increased initially. After the protrusion length reached a maximum, it steadily decreased; this indicates pore formation. Scale bar = 25 μm . Experiments A, B and C were repeated several times with similar results. (D) The protrusion length change was converted to $\Delta A/A$ for CAI (round dots, dashed lines) compared with controls (square dots and solid lines)—2 runs are shown for each. The osmolalities of the internal and external solutions of GUVs were initially balanced. The protrusion length increase in a control was due to water evaporation from the external solution. (E) $\Delta A/A$ vs. time for 4 runs of the NYAD-1 experiment. (F) $\Delta A/A$ vs. time for 3 runs of the NYAD-2 experiment. In (E, F), a decreasing $\Delta A/A$ is used to indicate pore formation, not a decrease in membrane area.

Figure 2 A GUV (DOPC) containing green dye calcein (MW 623) and red dye TRD (MW 10000) was in a solution of pH 7. NYAD-1 was injected slowly (a duration ~ 30 s) into the solution until it reached 25 μM . Time zero was at the beginning of peptide injection. The time of leakage depended on the distance between the injector and the GUV and the speed of injection; it should not be compared with Fig. 1B. Both dyes started to leak out at the same time. Scale bar = 50 μm .

Figure 3 (A) Confocal images of an aspirated GUV (DOPC) containing a pH 9 solution and 10 μM TRsc (red) in the lumen, first in the control chamber ($t < 0$) and then transferred to the observation chamber (time 0) containing a solution of 2 μM NYAD-2 (green) at pH 7. The binding of NYAD-2 (the green intensity on the GUV boundary increased with time) caused the membrane expansion (protrusion length increase) with no molecular leakage. (The bright, thin, horizontal red bar on the micropipette was an optical artifact.) Scale bar = 20 μm . (B) Relative intensities of fluorescence: Red for TRsc inside the GUV (normalized to one at $t = 0$); Black for the corrected solution intensity of NYAD-2 outside the GUV, I_0^c (also normalized to one at time=0); Green for the corrected intensity of NYAD-2 inside the GUV divided by the corrected intensity outside averaged over time, $\langle I_0^c \rangle$ (and divided by 1.78 due to the pH 9 effect): $I_t^f / (\langle I_0^c \rangle * 1.78)$. Note that the corrected intensity inside the GUV exceeded the corrected outside intensity after ~ 30 mins.

Figure 4 Permeation experiment in a pH 9 solution both inside and outside the GUV (DOPC). The top row shows the green channel images for the intensity of NYAD-2, and the bottom row

the red channel for the intensity of TR_{sc}. The observation chamber was sealed to keep the water from evaporation (hence no micropipette aspiration). The TR_{sc} intensity was essentially constant in 7 h. The inside to outside intensity ratios for NYAD-2, I_i^c/I_o^c , increased from a few percent in the first image to ~60% after ~7 h.

Figure 5 X-ray lamellar diffraction of NYAD-1/DOPC mixtures in a series of P/L. (A) Raw data of the diffraction patterns. (B) Electron density profiles of the bilayers: Z is the distance from the bilayer center. (C) The phosphate peak to phosphate peak distance across the bilayer, PtP, measured for a series of P/L. The error bars are that of reproducibility using two to three independently prepared samples.

Figure 6 OCD of NYAD-1 in a series of P/L and a solution CD for comparison. OCD spectra are mutually normalized to the same amount of peptide; the solution CD (red) was superimposed by matching long wavelength region to the OCD's. The OCD spectra imply that the NYAD-1 helices are parallel to the bilayer for $P/L \leq 1/20$. A fraction of NYAD-1 helices are oriented normal to the bilayer for $P/L \geq 1/15$.

Figure 1

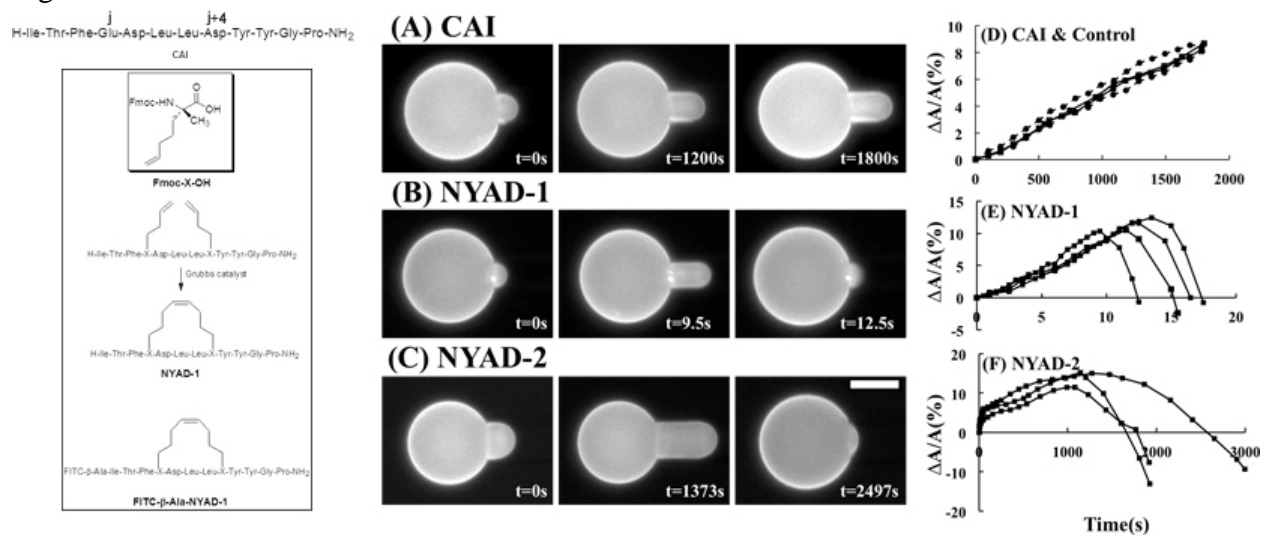


Figure 2

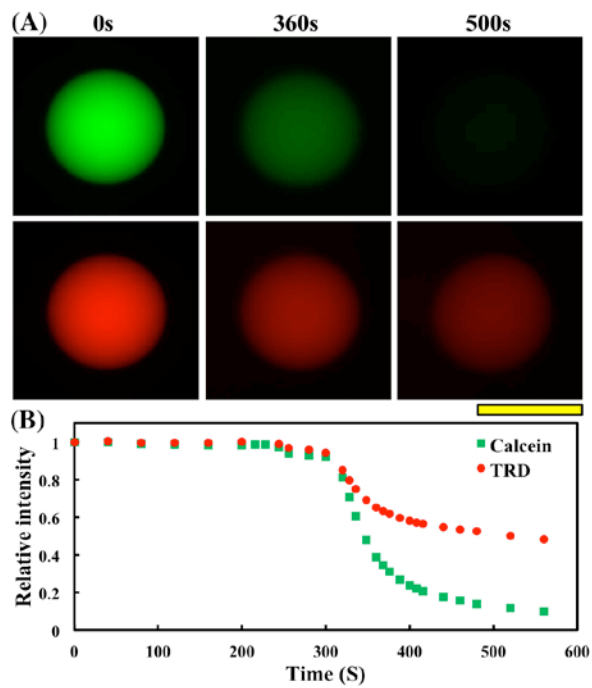


Figure 3

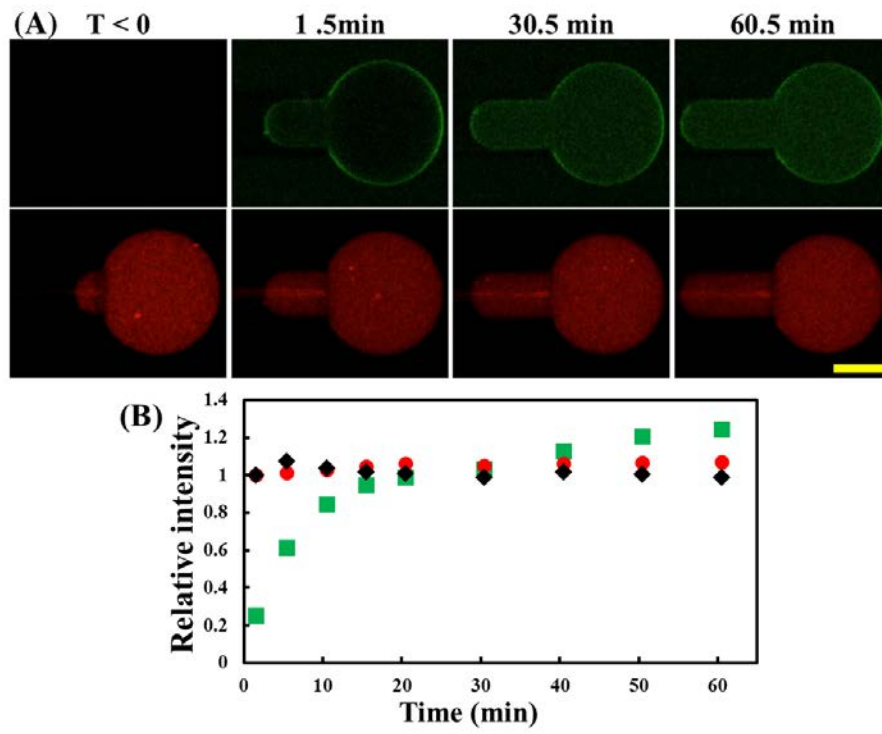


Figure 4

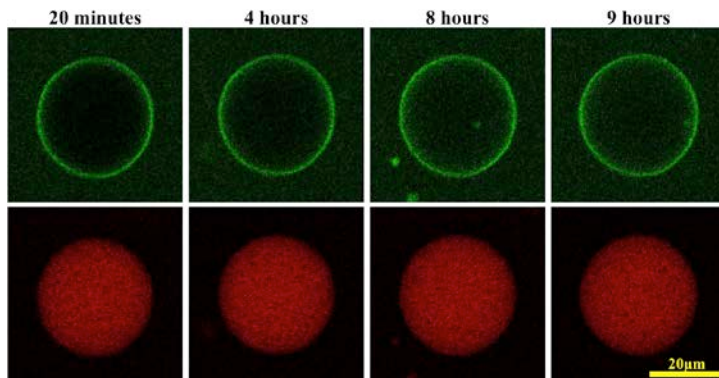


Figure 5

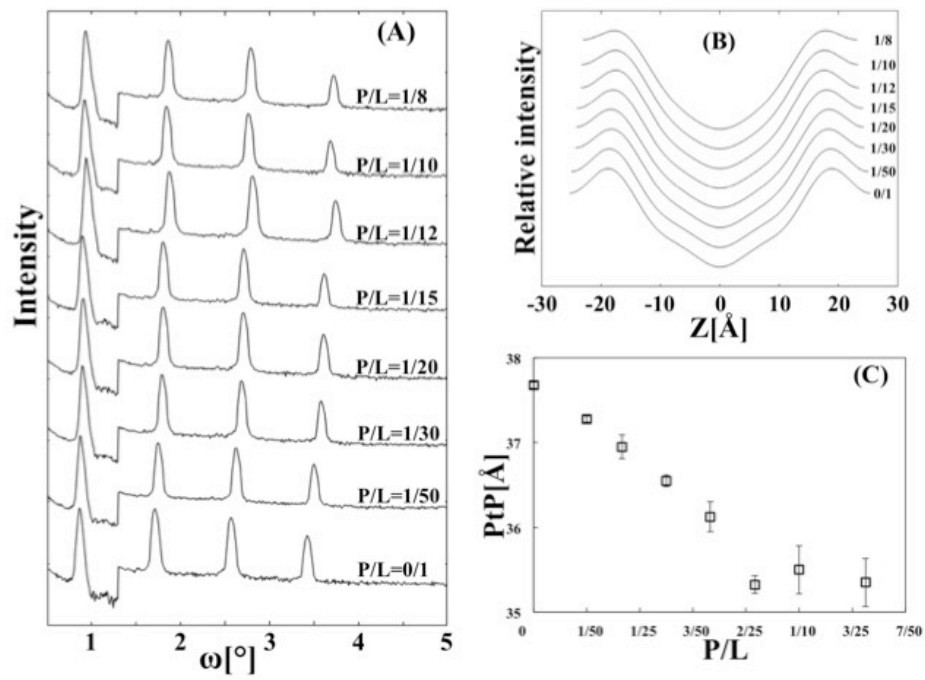


Figure 6

